

PAPER

Quantum engineering of Majorana quasiparticles in one-dimensional optical lattices

To cite this article: Andrzej Ptok *et al* 2018 *J. Phys.: Condens. Matter* **30** 355602

View the [article online](#) for updates and enhancements.

Related content

- [The Fulde–Ferrell–Larkin–Ovchinnikov state for ultracold fermions in lattice and harmonic potentials: a review](#)
Jami J Kinnunen, Jildou E Baarsma, Jani-Petri Martikainen *et al*.

- [Light-induced gauge fields for ultracold atoms](#)
N Goldman, G Juzelinas, P Öhberg *et al*.

- [Methods for detecting charge fractionalization and winding numbers in an interacting fermionic ladder](#)
Leonardo Mazza, Monika Aidelsburger, Hong-Hao Tu *et al*.



IOP | ebooks™

Bringing you innovative digital publishing with leading voices to create your essential collection of books in STEM research.

Start exploring the collection - download the first chapter of every title for free.

Quantum engineering of Majorana quasiparticles in one-dimensional optical lattices

Andrzej Ptok¹, Agnieszka Cichy^{2,3} and Tadeusz Domański⁴

¹ Institute of Nuclear Physics, Polish Academy of Sciences, ul. E. Radzikowskiego 152, PL-31342 Kraków, Poland

² Faculty of Physics, Adam Mickiewicz University, Umultowska 85, 61-614 Poznań, Poland

³ Institut für Physik, Johannes Gutenberg-Universität Mainz, Staudingerweg 9, D-55099 Mainz, Germany

⁴ Institute of Physics, Maria Curie-Skłodowska University, pl. M. Curie-Skłodowskiej 1, 20-031 Lublin, Poland

E-mail: aptok@mmj.pl, agnieszkakujawa2311@gmail.com and doman@kft.umcs.lublin.pl

Received 21 February 2018

Accepted for publication 27 July 2018

Published 13 August 2018




CrossMark

Abstract

We propose a feasible way of engineering Majorana-type quasiparticles in ultracold fermionic gases on a one-dimensional (1D) optical lattice. For this purpose, imbalanced ultracold atoms interacting by the spin–orbit coupling should be hybridized with a three-dimensional Bose–Einstein condensate molecular cloud. We show that the Majorana-type excitations can be created or annihilated upon constraining the profile of a trapping potential and/or an internal scattering barrier. This process is modeled within the Bogoliubov–de Gennes approach. Our study is relevant also to nanoscopic 1D superconductors, where both potentials can be imposed by electrostatic means.

Keywords: optical lattice, Majorana bound states, ultra cold Fermi gases

 Supplementary material for this article is available [online](#)

(Some figures may appear in colour only in the online journal)

1. Introduction

Ultracold quantum gases provide a unique opportunity for *quantum simulations* of interacting many-body systems [1]. Tremendous progress in experimental techniques in the last years has allowed to control all important ingredients of such simulations, giving an insight into physical mechanisms that eluded understanding in conventional, ‘natural’ condensed matter setups. In particular, both the depth of the periodic trapping potential and the lattice geometry can be controlled, offering a variety of opportunities for research [2]. Experiments in which fermionic or bosonic gases are loaded into the optical lattices have been carried out [3]. There has been significant experimental progress in the engineering of artificial gauge fields, the spin–orbit (SO) couplings or simulating non-Abelian fields [4–9].

Recent studies of topological matter, especially the topologically non-trivial superconductivity, are motivated by realization of exotic quasiparticle excitations that resemble Majorana fermions (MFs) [10–12]. In quantum field theory, MFs are particles that are their own antiparticles. In condensed matter, MF can be understood as a zero-energy quasiparticle which is its own ‘hole’. Moreover, Majorana excitations have an exotic exchange statistics—they are non-Abelian anyons [13–15], which makes them even more interesting. The prerequisites to observe such zero-energy Majorana modes in condensed matter systems are: a strong SO coupling, an external Zeeman magnetic field (population imbalance) and the existence of a gap in the energy spectrum [16–29]. The SO coupling is very important from the point of view of real systems. It determines the electronic structure of atoms but also leads to such non-standard phenomena as the emergence

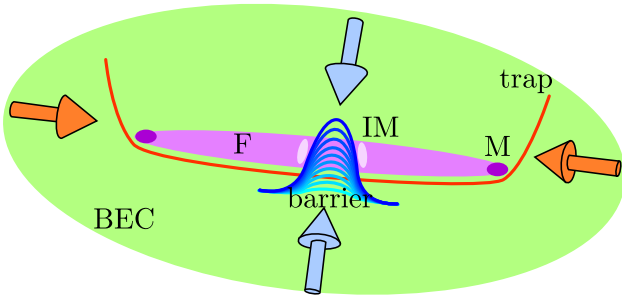


Figure 1. An ultracold fermionic gas loaded on a 1D lattice (F) coupled to a molecular BEC in a trap (the red line). The Majorana modes (M) are created on the edges of the wire. Placing inside the trap an additional potential barrier (blue lines), one can effectively split the fermionic chain, creating additional two edges, which causes the induction of extra Majorana states (IM).

of topological insulators. The SO coupling has been realized successfully in ultracold atomic gases setups. The first experimental realization of the SO coupling has been performed in Bose–Einstein condensate (BEC) using a two-photon Raman process [30] and one year later it has been reported for a fermionic gas [5, 31].

So far, various experimental methods for detecting Majorana quasiparticles have used either a semiconducting nanowire [17–23] or a magnetic chain [24–29] proximitized to superconductors, vortices in *p*-wave superconductors [32–36], or some lithographically designed nanostructures [37]. Finding feasible means for manipulating Majorana *quasi*-particles in such systems is still a big challenge. We address this issue for a nonuniform 1D system, where an additional pair of Majorana modes can be controllably created by designing a proper internal scattering potential.

Our present study is inspired by the proposal of Jiang *et al* [16] to investigate a trapped spin-imbalanced fermionic gas on a 1D optical lattice. This fermionic system is coupled to a 3D molecular BEC cloud (figure 1), which provides the on-site *s*-wave pairing of atoms. By applying the spin–orbit and the Zeeman interactions (via a synthetic magnetic field), *p*-wave pairing can be induced between same-spin atoms on neighboring sites [7, 38–41] leading to a topologically non-trivial superconducting state, manifested by zero-energy Majorana bound states (MBS). Similar ideas have been considered for two-dimensional *p*-wave superfluids of fermionic atoms in optical lattices [42], where Majorana modes could appear as topological defects, such as vortices or edges of lattice dislocations, which take the form of one-dimensional wires.

The main objective of the paper is to investigate how the energy spectrum of a 1D fermionic system (in particular containing MFs) can be controllably influenced by an internal scattering potential, sketched by the blue lines in figure 1. We have checked that the curvature of the harmonic trapping potential has important influence on realization of the topological phase and on the number of Majorana modes. The paper is organized as follows. In section 2, we introduce the theoretical model for our system and discuss its characteristic properties. In section 3, we present numerical results obtained by the Bogoliubov–de Gennes treatment, considering the Majorana modes gradually induced at the internal potential

barrier. Finally, in section 4, we summarize the results and give a brief outlook.

2. Model and technique

The 1D atomic Fermi chain on an optical lattice and coupled to a 3D molecular BEC (figure 1) can be described by the following Hamiltonian:

$$\mathcal{H} = \mathcal{H}_0 + \mathcal{H}_{SO} + \mathcal{H}_{BEC} + \mathcal{H}_{trap} + \mathcal{H}_{bar}. \quad (1)$$

Here, $\mathcal{H}_0 = \sum_{i,j\sigma} (-t\delta_{ij}) - (\mu + \sigma h) \delta_{ij} c_{i\sigma}^\dagger c_{j\sigma}$ describes free fermionic atoms on the lattice, which hop between the nearest-neighbor sites with the hopping amplitude t , $\sigma \in \{\uparrow, \downarrow\}$ is the spin index, μ —the chemical potential and h is a Zeeman field which originates from a population imbalance. Experimentally, such population imbalance between two different fermionic mixtures is quite easy to obtain, because the populations in two hyperfine states of the fermionic atom can be freely chosen [43–45]. Usually, a degenerate Fermi gas of spin-polarized atoms is prepared using the standard techniques of laser cooling, sympathetic cooling by sodium atoms, and optical trapping [43]. The spin–orbit coupling can be expressed by $\mathcal{H}_{SO} = -i\lambda \sum_{i\sigma\sigma'} c_{i\sigma} (\hat{\sigma}_y)_{\sigma\sigma'} c_{i+1\sigma'} + \text{h.c.}$, where $\hat{\sigma}_y$ is the Pauli *y*-matrix. To create electromagnetic fields for neutral atoms, an artificially produced vector potential has to be applied to the atoms. In the presence of an artificially generated gauge field, neutral ultracold atoms act in the same way as a charged particle would in the presence of a magnetic field. By engineering spatially-dependent complex tunneling amplitudes with laser-assisted tunneling and a potential energy gradient, two independent research groups have reported compelling evidence for the realization of the Hofstadter Hamiltonian with neutral rubidium atoms that are loaded into laser-induced periodic potentials [46, 47]. Coupling of the BEC with the fermionic chain leads to the proximity induced on-site pairing, which can be effectively modeled as $\mathcal{H}_{BEC} = \sum_i (\Delta c_{i\downarrow} c_{i\uparrow} + \text{h.c.})$. Δ plays the role of the effective gap induced in the fermionic chain by the BEC background. Formally, $\Delta \approx g\Xi$ [16], where g denotes the coupling constant between the composite bosonic and fermionic mixtures, whereas Ξ corresponds to macroscopic occupation in the ground state by composite bosons in the BEC [48]. $\mathcal{H}_{trap} = \sum_{i\sigma} V(i) c_{i\sigma}^\dagger c_{i\sigma}$ corresponds to the trapping potential, whereas $\mathcal{H}_{bar} = \sum_{i\sigma} \Lambda(i, \tau) c_{i\sigma}^\dagger c_{i\sigma}$ describes the potential barrier inside the trap at time τ . The specific form and role of both these potentials is described in section 3.

2.1. Bogoliubov–de Gennes formalism

The quasiparticle spectrum of ultracold atoms described by the Hamiltonian \mathcal{H} can be obtained from a diagonalization procedure based on the canonical transformation

$$c_{i\sigma} = \sum_n (u_{in\sigma} \gamma_n - \sigma v_{in\sigma}^* \gamma_n^\dagger), \quad (2)$$

where γ_n and γ_n^\dagger are the quasiparticle fermionic operators. The coefficients $u_{in\sigma}$ and $v_{in\sigma}$ fulfill the Bogoliubov–de

Genness (BdG) equations $\mathcal{E}_n \Psi_{in} = \sum_j \mathbb{H}_{ij} \Psi_{jn}$ [49], where $\Psi_{in} = (u_{in\uparrow}, u_{in\downarrow}, v_{in\downarrow}, v_{in\uparrow})$ is a four-component spinor, and the matrix is defined as

$$\mathbb{H}_{ij} = \begin{pmatrix} H_{ij\uparrow\uparrow} & H_{ij\uparrow\downarrow} & \Delta_{ij} & 0 \\ H_{ij\downarrow\uparrow} & H_{ij\downarrow\downarrow} & 0 & \Delta_{ij} \\ \Delta_{ij}^* & 0 & -H_{ij\downarrow\downarrow}^* & H_{ij\downarrow\uparrow}^* \\ 0 & \Delta_{ij}^* & H_{ij\uparrow\downarrow}^* & -H_{ij\uparrow\uparrow}^* \end{pmatrix}, \quad (3)$$

where $H_{ij\sigma\sigma'} = (-t\delta_{\langle ij \rangle} - (\bar{\mu}(i, \tau) + \sigma h)\delta_{ij})\delta_{\sigma\sigma'} + H_{SO}^{\sigma\sigma'}$ and $\Delta_{ij} = \Delta\delta_{ij}$. Here $\bar{\mu}(i, \tau) = \mu - V(i) - \Lambda(i, \tau)$ is an *effective* local chemical potential on site i and at time τ . We introduce the following spin-orbit terms: $H_{SO}^{\uparrow\downarrow} = \lambda(\delta_{i+1j} - \delta_{i-1j})$, $H_{SO}^{\uparrow\uparrow} = H_{SO}^{\downarrow\downarrow} = 0$ and $H_{SO}^{\downarrow\uparrow} = (H_{SO}^{\uparrow\downarrow})^*$.

It is important to emphasize that one of the greatest advantages of the BdG method is the possibility of diagonalization of the Hamiltonians which describe inhomogeneous systems. The BdG formalism consists in solving the Bogoliubov–de Gennes self-consistent equations. However, the order parameter (e.g. the superconducting order parameter Δ_i) is defined locally, i.e. for a given site i and it depends on all possible states described by the Hamiltonian.

The realization of ultracold lattice systems in a trapping potential introduces inhomogeneity to the system, which is effectively expressed as an extra ‘*chemical potential*’ with parabolic dependence on the distance from the center of the trap $\mathcal{H}_{\text{trap}}$ [50–54]. Hence, this method is a natural choice to provide a qualitative analysis of the system studied in this work.

2.2. Signatures of Majorana quasiparticles

MBS exist only in the topologically non-trivial superconducting phase and they represent the zero-energy modes, $\mathcal{E}_n = 0$. One needs to remember that only these states exactly fulfill the condition: $\gamma_n = \gamma_n^\dagger$, which is the defining property of Majorana quasiparticles. For detecting them in the system, the following quantities can be considered: (i) the local density of states (LDOS) [55], (ii) the density of Majorana quasiparticles \mathcal{P}_M [56], and (iii) the topological quantum number \mathcal{Q} [57]. Below, we briefly point out their physical importance.

The LDOS of fermionic atoms in a given site i is defined as $\rho(i, \omega) = -1/\pi \sum_\sigma \text{Im} G_{i\sigma, 11}(\omega + i0^+)$, where $G_{i\sigma}(\omega) = (\omega - \mathbb{H})^{-1}$ is the single particle Green’s function with the matrix \mathbb{H} given in equation (3). Applying the transformation (2), LDOS can be expressed as [58, 59]:

$$\rho(i, \omega) = \sum_{n, \sigma} [|u_{in\sigma}|^2 \delta(\omega - \mathcal{E}_n) + |v_{in\sigma}|^2 \delta(\omega + \mathcal{E}_n)], \quad (4)$$

where $\delta(\omega)$ is the Dirac delta function and \mathcal{E}_n is determined by the BdG equations.

The appearance of the zero-energy MBS can be observed as a zero-energy peak in the scanning tunneling microscopy (STM) or differential conductance measurements [60–66]. In the condensed matter systems, MBS are created at the edge of a nanowire given by the gate potential. In theoretical calculations, this potential is modeled by e.g. the Gaussian

profile [60] or hard-wall boundaries [66]. In turn, in ultracold fermionic mixtures, trapping/barrier potential can be tuned by the parameters of the optical lattices [67], in a relatively simple way. In this system, the LDOS measurements can be performed using the radio-frequency (*rf*) spectroscopy, which is an analog of STM measurements [17, 24, 68–73]. This technique has been successfully used in the in-gap state measurements [74, 75]. Additionally, because of the fact that MBS are formed in the system with non-zero magnetization (polarization), this bound state can be detected as a polarized zero-energy localized state, at the edge of the system [29]. As a consequence, MBS can also be detected by spin-dependent techniques [76].

The density of Majorana quasiparticles \mathcal{P}_M is characterized by the off-diagonal spectral function at zero energy [56]:

$$\mathcal{P}_M(i) = \sum_n |u_{in\downarrow} v_{in\downarrow}^* - u_{in\uparrow} v_{in\uparrow}^*| \delta(\mathcal{E}_n). \quad (5)$$

This quantity is helpful for investigating non-locality of the Majorana quasiparticles. For numerical calculations of equations (4) and (5), we have replaced the Dirac delta function by a narrow Lorentzian $\delta(\omega) = \zeta/[\pi(\omega^2 + \zeta^2)]$ with a broadening $\zeta = 0.002$ for $\rho(i, \omega)$ and $\zeta = 10^{-12}$ for $\mathcal{P}_M(i)$.

Another important physical quantity is the topological number $\mathcal{Q} = (-1)^m$, which is determined by the parity of the number m of Majorana bound states at each edge of the wire [10]. This quantity is helpful for identification of the topological nature of the system. \mathcal{Q} can be obtained from the scattering matrix \mathcal{S} , which describes the relation between incoming and outgoing wave amplitudes at the Fermi level [57]:

$$\begin{pmatrix} \psi_{-L} \\ \psi_{-R} \end{pmatrix} = \mathcal{S} \begin{pmatrix} \psi_{+L} \\ \psi_{+R} \end{pmatrix}, \quad \mathcal{S} = \begin{pmatrix} R & T' \\ T & R' \end{pmatrix}, \quad (6)$$

where $\psi_{+,i}$, $\psi_{-,i}$ denote incoming and outgoing mode amplitudes, respectively. The \mathcal{S} matrix is built from blocks of reflection R, R' and transmission T, T' matrices at the two ends of the system. Here, we determine \mathcal{Q} within the BdG approach from the sign of the scattering matrix, $\mathcal{Q} = \text{sgn det}(R) = \text{sgn det}(R')$. The numerical procedure is discussed in [77]. Formally, \mathcal{Q} is defined by the Pfaffian of R and can be treated as the spin Chern number for the \mathbb{Z}_2 topological phase [78, 79]. Several methods for numerical determination of the topological quantum number have been proposed in the literature [80–82]. Particularly interesting is the odd fermion parity, $\mathcal{Q} = -1$, referring to the topologically nontrivial superconducting phase [83, 84], which supports the realization of MBS.

2.3. Symmetry class

In the case of open boundary conditions, bound states emerge at the end of the system. However, the information about possibility of the realization of the non-trivial topological state can be taken from the system with periodic boundary conditions. In our case, for the homogeneous system (with periodic boundary conditions), the Hamiltonian $\mathcal{H}' = \mathcal{H}_0 + \mathcal{H}_{SO} + \mathcal{H}_{\text{BEC}}$ can be rewritten in the form:

$$\mathcal{H}' = \sum_k \Phi_k^\dagger \mathcal{H}_k \Phi_k, \quad \mathcal{H}_k = \begin{pmatrix} H_k & \hat{\Delta} \\ \hat{\Delta}^* & -H_{-k}^* \end{pmatrix}, \quad (7)$$

where $\Phi_k^\dagger = (c_{k\uparrow}^\dagger, c_{k\downarrow}^\dagger, c_{-k\downarrow}, c_{-k\uparrow})$ is the Nambu spinor in momentum space ($c_{k\sigma}$ denotes the annihilation operator of electron with momentum \mathbf{k} and spin σ). Here, H_k and $\hat{\Delta}$ denote the matrix forms of the Fourier transform of $\mathcal{H}_0 + \mathcal{H}_{\text{SO}}$ and \mathcal{H}_{BEC} terms, respectively:

$$H_k = \begin{pmatrix} \xi_{k\uparrow} & \mathcal{L}_k \\ \mathcal{L}_k^* & \xi_{k\downarrow} \end{pmatrix}, \quad \hat{\Delta} = \begin{pmatrix} \Delta & 0 \\ 0 & \Delta \end{pmatrix}, \quad (8)$$

with $\xi_{k\sigma} = -2t \cos(k) - (\mu + \sigma h)$ as a dispersion relation and $\mathcal{L}_k = -2i\lambda \sin(k)$ spin-orbit coupling in momentum space.

Using the Hamiltonian in the form (7), we can find the symmetry class of the system under consideration [85]. The particle-hole symmetry (PHS) is always conserved in the BdG-type Hamiltonian [86], $U_P \mathcal{H}_k^* U_P^{-1} = -\mathcal{H}_{-k}$, with the PHS operator $P = U_P K$. Here, K is the complex conjugate operator, $U_P = \hat{\sigma}_x \otimes \hat{\sigma}_0$ and $P^2 = 1$. In a similar way, we can define the time reversal symmetry (TRS) with the TRS operator $T = U_T K$, where $U_T = \hat{\sigma}_0 \otimes i\sigma_y$, and $T^2 = -1$. In this case, in the absence of the magnetic field, the Hamiltonian satisfies TRS, and $U_T \mathcal{H}_k U_T^{-1} = \mathcal{H}_{-k}$. According to the symmetry classification, the system belongs to the DIII class [87]. However, the external magnetic field leads to the breaking of TRS and changes the symmetry class from DIII to D. It should be mentioned that the 1D system with the class D is described by the \mathbb{Z}_2 invariant (defined in the previous paragraph) and it allows for the realization of the pair zero-energy mode at the edge of the system.

3. Numerical results and discussion

The dispersion relation for a homogeneous 1D chain with the strong SO coupling and the Zeeman splitting is displayed in figure 2(a). For the topologically trivial phase, the degeneracy of the Fermi level μ_1 is fourfold, whereas in a topologically non-trivial phase the Fermi level μ_2 has only two-crossing points [19]. By varying the chemical potential μ , the system qualitatively changes from the topologically non-trivial to topologically trivial one (figure 2(b)). In the first case, i.e. in the region located to the left of point A and to the right of point B, there is the standard gapped spectrum. However, between the point A and B in figure 2(b), there exists a topologically non-trivial phase, which is manifested by the zero-energy MBS that is topologically protected inside the gap (the red line in figure 2(b)). Such a topological phase occurs when $h > \sqrt{\Delta^2 + (2t \pm \mu)^2}$ [39, 40, 88], thereby depending on the chemical potential (see μ_2 in figure 2(b)). Due to this fact, we choose the following model parameters: $h = 0.3t$, the SO coupling $\lambda = 0.15t$ and the gap $\Delta = 0.2t$. For our calculations, we considered a system consisting of $N = 600$ sites.

3.1. Role of the external trapping potential

Any trapping potential $V(i)$ leads to inhomogeneous distribution of the particles [44, 45, 89–92]. In this case, the MBS

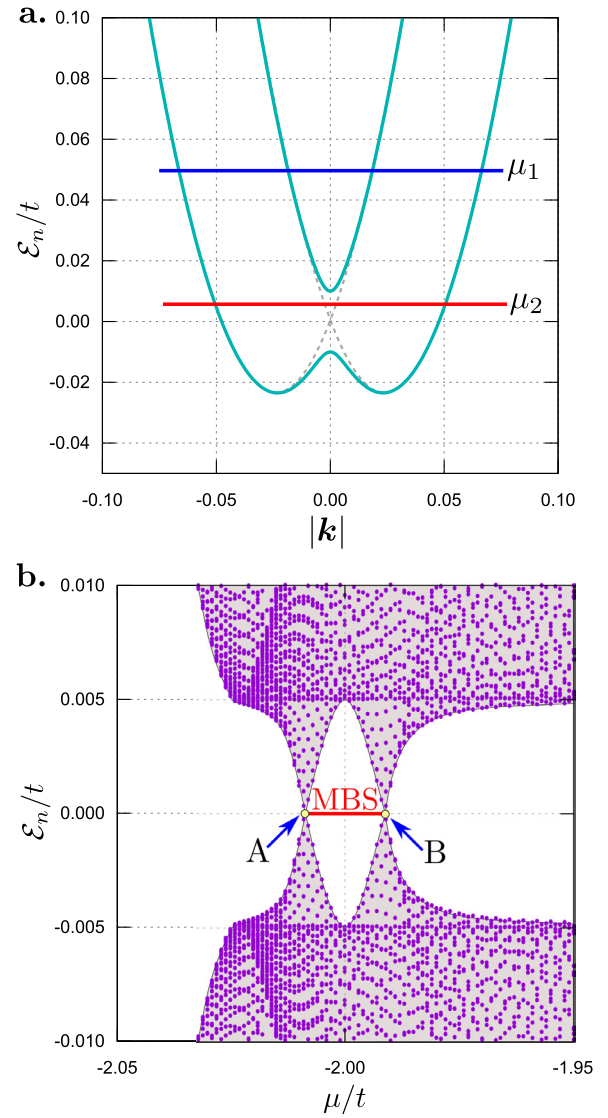


Figure 2. Numerical results for (a) the dispersion relation for the non-interacting system, described by the Hamiltonian H_k (8) and (b) the spectrum of the system, described by the Hamiltonian \mathcal{H}' (7). (a) The BEC medium induces pairing between opposite momenta and spin states, which creates a gap of size Δ . For the Fermi level μ_1 (μ_2), the topologically (non-)trivial phase is realized. (b) Spectrum of the Hamiltonian versus the chemical potential μ . The red line illustrates Majorana bound states, topologically protected inside the energy gap, occurring between A and B, which determine the boundary of the topologically non-trivial phase. Results in the absence of the trap and barrier potential, for $\lambda/t = 0.15$, $\Delta/t = 0.005$ and $h/t = 0.01$.

appear on the boundaries of the topologically non-trivial superconducting phase. In our study, we considered the trapping potential of: (i) the parabolic $V(i) = V_0(r_i - r_{N/2})^2$ and (ii) the Gaussian shape at the 1D lattice edges, $V(i) = V_0 [\exp(-r_i^2/2\sigma^2) + \exp(-r_{N-i}^2/2\sigma^2)]$. Without much loss of generality, we assumed the internal barrier potential of the Gaussian shape $\Lambda(i) = \Lambda_0(\tau) \exp(-(r_i - r_{N/2})^2/2\sigma^2(\tau))$. Here, $r_{N/2}$ corresponds to the central point of the trap. The parameters Λ_0 and σ characterize the height and the width of the interior potential, respectively.

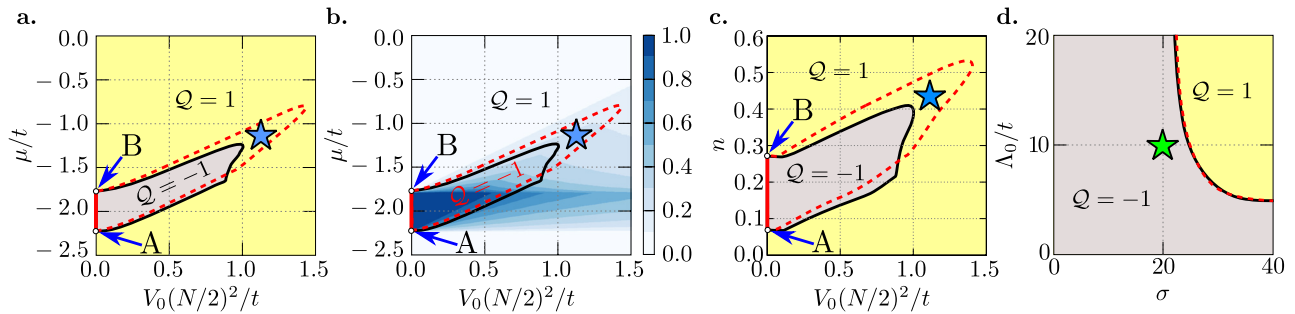


Figure 3. The phase diagram obtained for the harmonic trap $V_0\delta r^2$ ((a)–(c)) and for the Gaussian-like potential $\Lambda_0 \exp(-\delta r^2/2\sigma^2)$ (d), where δr is the distance from the center of the system and σ is the potential width. The solid black lines and the dashed red lines show the boundaries of the topological phase, which supports the realization of Majorana quasiparticles $\mathcal{Q} = -1$, in the case of the system with $N = 600$ and 900 sites, respectively. The trivial phase corresponds to $\mathcal{Q} = 1$. Panels (a) and (b) show the chemical potential μ or (panel (c)) the average number of particles n versus the potential at the edge of the trapping potential, in the case of the harmonic trap. Background color in panel (b) shows the ratio of the sites being in the local topological phase to the total number of sites in the lattice. The results are obtained at fixed $h = 0.3t$. Panel (d) shows how the parameters Λ_0 and σ of the Gaussian potential affect the topological phase. The results are obtained at fixed $\mu = -2.18t$ and $h = 0.3t$. The green star shows the values of parameters used in our calculations. The blue star in the panels ((a)–(c)) indicates the region for which the strong influence on the size system appears, whereas the red line between A and B points illustrates the region of parameters in the case of the finite homogeneous system (without a boundary condition) in which the Majorana bound states can exist.

A possible realization of topological superfluids in 1D spin-orbit coupled Fermi gases trapped by a harmonic potential has been considered quite recently [54, 93–95]. In these systems, both the pairing gap $\Delta(i)$ and the effective chemical potential $\bar{\mu}(i, \tau)$ were assumed to be spatially dependent [54, 92–95]. Consequently, the occurrence of the topological phase was predicted *locally* for such regions of the trap, for which the following condition is fulfilled: $h > \sqrt{\Delta^2(i) + (2t + \bar{\mu}(i, \tau))^2}$, at time τ . Under specific conditions, a topological superfluid can appear at the trap edges, whereas a conventional superfluid is present around the trap center [54, 92, 93]. For creating the Majorana quasiparticles in the central part, some additional constraints were proposed, for instance by introducing a magnetic impurity [93] or using dark solitons [94, 95] that locally change $\Delta(i)$ and/or $\bar{\mu}(i, \tau)$.

In our system, the atoms are coupled to the BEC background with a constant pairing gap Δ . The trapping and/or barrier potentials have crucial influence on the transition between the topologically trivial and non-trivial phases, signaled by a change of the topological number \mathcal{Q} (defined in section 2). The topological region $\mathcal{Q} = -1$ (supporting MBS) is depicted by gray color in the phase diagrams of figure 3.

Let us start the discussion with the harmonic potential case, $V(i) = V_0(r_i - r_{N/2})^2$ (figures 3(a)–(c)). As a natural energy scale of the fermion atomic system, we choose a value of the trapping potential on the first or the last site (given by $V_0(N/2)^2$)⁵. This allows us to compare the results for different sizes N of the system. In figures 3(a)–(c), we present the results obtained for $N = 600$ (solid black lines) and for $N = 900$ sites (dashed red lines). For a very flat parabolic shape (small V_0) of the trap, we observe that the topological phase exists for comparable ranges of parameters (at fixed h) in both cases.

⁵ Another relevant energy scale would be a value of the trapping potential at the Fermi radius, understood as a distance from the center of the trap to the last occupied site [96]. However, its numerical determination is more complicated.

Some deviations show up when the trapping potential is more steep. We explain this effect below.

In the absence of the trap ($V_0 = 0$), our results are identical with those obtained for the homogeneous system. In this case, the topological phase is marked in figures 3(a)–(c) by the solid red line between points A and B, whereas A and B points indicate boundaries of the topological phase mentioned when discussing figure 2. This system is analogous to the nanowire system realized experimentally in solids and mentioned in section 1. In ultracold gasses, this situation formally corresponds to a quantum well with an infinite barrier at its edges.

Any non-zero value of V_0 affects the regime in which MBS can be realized. This is a consequence of the *local* modifications of the topological phase. The change of the effective chemical potential $\bar{\mu}(i, \tau)$ leads to the situation that not every site in the system fulfills the constraint $h > \sqrt{\Delta^2 + (2t + \bar{\mu}(i, \tau))^2}$. Therefore, the topological phase can vanish on some sites. This is clearly visible in figure 3(b), which shows the ratio of the optical lattice sites obeying the above condition to the total number of sites. We notice that the topological phase forms *locally* around the chemical potential $\mu \sim -2t$ and, with increasing V_0 , moves towards higher values of μ . For very steep curvature of the harmonic trap, the topological phase disappears. In this case, the extreme decrease of the Fermi radius can be observed and the reduction of the distance between MBS localized around it takes place (around blue star). As a result, the possibility of an overlap increases and depends on the Fermi radius (which here is defined as a half-distance between the MBS). It is comparable with the case in which MBS are localized at the end of a long 1D lattice. Then, the spatial extension of the Majorana wavefunction ζ_M (i.e. the characteristic length which describes the exponential decay of the MBS in space [97]) is comparable with the superconducting coherence length ζ_c (i.e. the Cooper pair size) [98]. If the distance between the Majorana wavefunctions (i.e. the distance between the maxima of Majorana wavefunctions) is too small (smaller than ζ_c), then

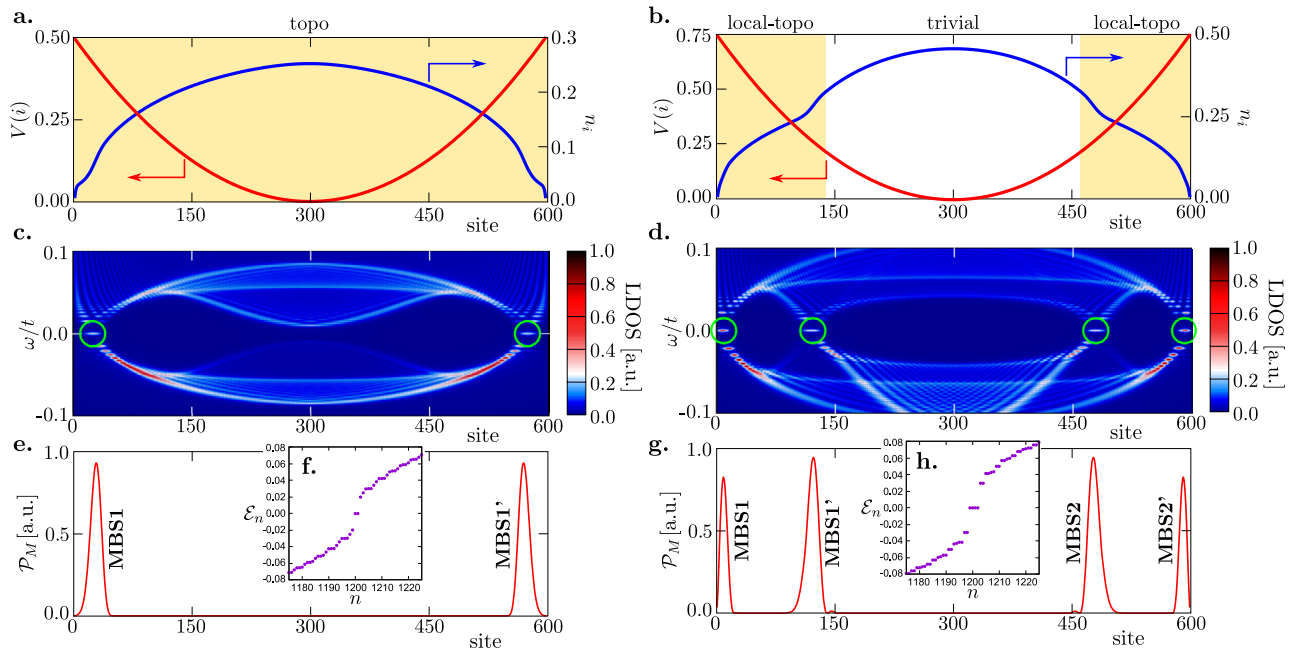


Figure 4. Examples of an influence of the harmonic trapping potential on the realization of the topological phase in the 1D system with $N = 600$ sites. The left column shows the results for $V_0(N/2)^2/t = 0.5$, $\mu = -1.8t$ and the right one for $V_0(N/2)^2/t = 0.75$, $\mu = -1.5t$, respectively. Panels (a) and (b) display the spatial profiles of the trapping potential V_i (red solid line) and the distribution of particles n_i (blue solid line). Panels (c) and (d) illustrate the local density of states, whereas panels (e) and (g)—the Majorana density \mathcal{P}_M . Insets (f) and (h) show the eigenvalues of (3) around the zero energy. Green circles at panels (c) and (d) show the place where the Majorana quasiparticles are localized.

the Majorana quasiparticles wave functions around the Fermi radius interfere with each other and, as a consequence, MBS is not observed. As a consequence, we observe the typical near zero-energy Andreev bound states with an exponentially small energy $\sim \exp(-L/\zeta_M)$ [95, 99].

In the case of a fixed total number of atoms, changes of the V_0 parameter modify the *effective* chemical potential $\bar{\mu}(i, \tau)$, thereby affecting the spatial profile of particles per site, $n_i = n_{i\uparrow} + n_{i\downarrow}$, where the number of particles per site is given by

$$n_{i\sigma} = \langle c_{i\sigma}^\dagger c_{i\sigma} \rangle = \sum_n (|u_{in\sigma}|^2 f(\mathcal{E}_n) + |v_{in\sigma}|^2 f(-\mathcal{E}_n)), \quad (9)$$

where $f(\omega) = 1/(1 + \exp(\omega/k_B T))$ is the Fermi–Dirac distribution. When systems differ in size N , the trapping potential curvature V_0 yields a different Fermi radius. As a consequence, the boundaries of the topological phase can depend on the size of the system (compare the black solid line with the red dashed line in figures 3(a)–(c)). Using the mapping of the chemical potential μ onto the average number of particles, $n = 1/N \sum_i n_i$, we can see how the shape of the trap influences the topological phase in real systems, in which the number of particles is fixed. When the average concentration n is fixed in the range between A and B points (the solid red line), then upon increasing the amplitude V_0 , the system evolves from the topological to the trivial superconducting phase. However, for fillings n above point B in the diagram, reentrant transitions are possible—from the trivial to the topological as well as from the topological to the trivial phase.

To illustrate this situation, we show numerical results for two cases: (i) when the whole system is in the topological phase and, (ii) when only a part of the system is in the topological phase (see the left and right panels in figure 4). For both cases, the Fermi radius is comparable to the system size. In the first case, when all sites are in the topological phase (marked by dark yellow background color in panel (a)), only one pair of MBS is created on the edges of the system (i.e. there are only two eigenvalues with zero energy—see panel (f)). This is also visible in LDOS (panel (c)) or the Majorana density (panel (e)). Situation changes in the case when the shape of the trapping potential allows for two *locally* separated topological regions, nearby the edge of the system, while the central part remains in the trivial phase (panel (b)). Under such circumstances, there appears one pair of MBS in each topological region, as reported in [54, 92–95]. We then obtain four-fold degeneracy of the zero-energy eigenvalue (panel (h)).

We also studied the Gaussian trapping potential (figure 3(d)), investigating for which combinations of parameters Λ_0 and σ the topological phase occurs. A trapping potential in this form can be regarded as a quantum well with smooth edges. As a consequence, for chosen range of parameters, the Gaussian potential allows for the topological superconductivity without any phase separation. For extremely small σ (i.e. very steep borders of the trapping potential), the system resembles a uniform nanowire of a finite length, which (at fixed value of the chemical potential and the magnetic field) is in the topological phase. Upon increasing the width σ , one observes that the range of the topological phase shifts to the smaller amplitude Λ_0 of the Gaussian trapping potential (which effectively

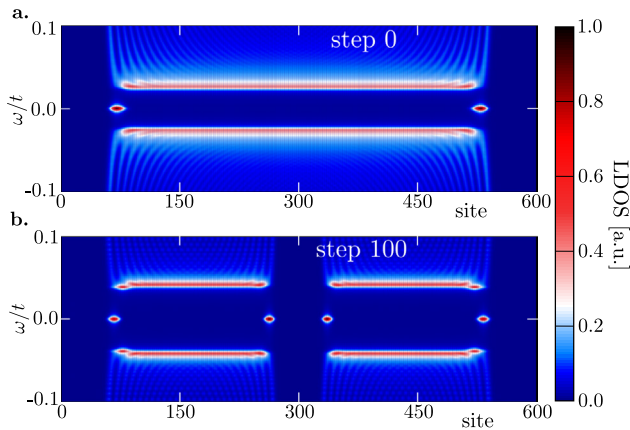


Figure 5. The spatially-dependent spectrum of fermionic atoms in the Gaussian trap at time step 0 (a) and with the internal barrier, after the creation of an additional pair of Majorana bound states at time step 100 (b).

corresponds to changes of the average number of particles in the quantum well with non-homogeneous edge). In this case, changeover from the topological to the trivial phase depends on the choice of parameters. For further analysis we studied the trapping potential of the Gaussian form (with flat bottom and the Gaussian distribution boundary shape), using $\Lambda_0 = 10t$ and $\sigma = 20$ (marked by the green star in figure 3(d)).

3.2. Majorana quasi-particles driven by internal scattering barrier

We discuss now the gradual emergence of additional (internal) Majorana quasiparticles induced by the scattering potential centered at a bottom of the confining potential. To visualize such process, we assumed time-dependent parameters Λ_0 and σ and studied ‘non-Markovian’ evolution of the quasiparticle spectrum, assuming that at each time step τ the system is in an equilibrium configuration that is achieved adiabatically. In other words, the actual configuration depends solely on the scattering potential at a given step τ . It should be mentioned that more realistic Markovian evolution can be considered using e.g. the *Floquet formalism* [16, 100–104] or the *Keldysh formalism* [105, 106]. However, this issue is beyond the scope of our present study.

We assumed that the scattering potential evolves in the following way: in region \mathcal{A} , the height Λ_0 increases with a fixed broadening σ and in region \mathcal{B} , the width σ increases keeping a constant height Λ_0 . For specific computations, we imposed $\Lambda_0(\tau) = 5\tau/75$, $\sigma(\tau) = 5$ (for $\tau < 75$), and $\Lambda_0(\tau) = 5$ and $\sigma(\tau) = 5 + (\tau - 75)/4$ (for $\tau \geq 75$), respectively⁶. In both cases, the system is in the topologically non-trivial superconducting state. We kept the fixed concentration $n \simeq 0.16$ ($T = 0$) of atoms by tuning the chemical potential, which varied rather insignificantly in the interval $\tau \in (0, 100)$. This concentration yields $\mu \simeq -2.18t$ in the first step, which satisfies the condition for realization of the topological

⁶ See supplemental material pot.mp4 available online at stacks.iop.org/JPhysCM/30/355602/mmedia for an illustration of the changes in a profile of the trapping potential.

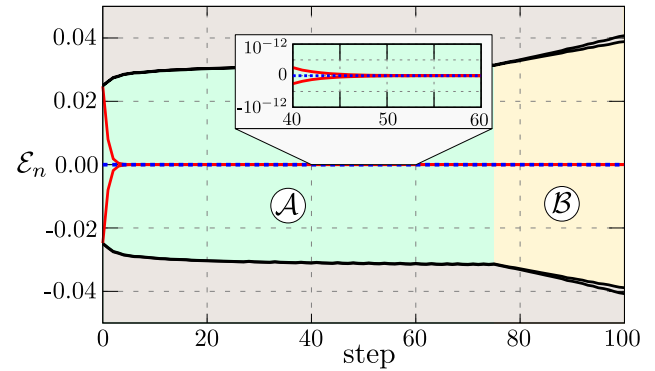


Figure 6. Evolution of the low-energy eigenvalues of the system (3) with respect to the varying potential barrier, for the parameters described in the main text. Region \mathcal{A} refers to an increasing height of the barrier amplitude and region \mathcal{B} to a widening of the barrier, respectively. The dotted blue (solid red) lines correspond to the quasiparticles at the external boundary (internal barrier) potential. The grey area denotes the region of the ordinary (finite-energy) Andreev bound states. The inset displays a zoom of the main figure for steps (40; 60), at which the internal Majorana modes are created.

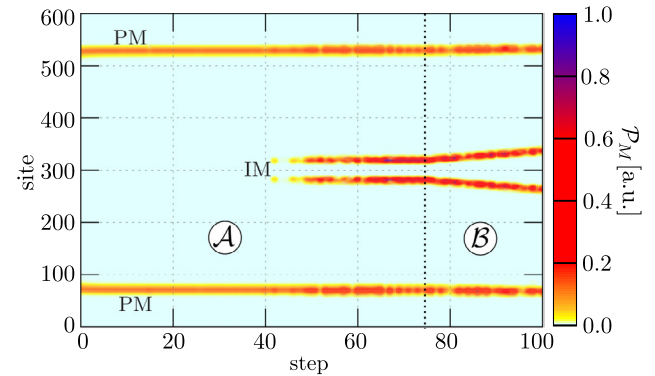


Figure 7. Density of the Majorana states \mathcal{P}_M for a varying barrier potential. The primary (PM) and induced Majorana quasiparticles are at the edges of the trapping potential and near the internal barrier, respectively.

superconducting phase. Under such conditions, the MBS on both sides of the system appear.

For the varying scattering barrier⁷, we determined the spatially dependent spectrum (4), starting from the situation with one pair of edge MBS (figure 5(a)). Such evolving scattering potential gradually induced the internal pair of the MBS, close-by to the internal barrier. The final spectrum of the system (at time step 100) is displayed in figure 5(b).

By investigating the low-energy eigenvalues of the system (figure 6), we noticed that two Andreev states tend to form the Majorana quasiparticles already from the 5th step onwards. Such peaks, however, do not correspond to the zero-energy of the quasiparticles. For recognizing the *true* Majorana modes and spotting their spatial localization, one can use the density $\mathcal{P}_M(i)$, which distinguishes the Majorana from the ordinary Andreev states [107, 108]. Let us remark that the

⁷ See supplemental material ldos.mp4 for an illustration of the evolution of a spatially-dependent spectrum of the fermionic atoms in the Gaussian trap.

zero-energy quasiparticles can be induced by a disorder or by the Kondo effect, so it is very important to properly identify the Majorana modes [22]. Figure 7 shows the numerical results for $\mathcal{P}_M(i)$, where the *true* Majorana⁸ modes gradually emerge around $\tau \approx 45$ (see inset in figure 6), where the Majorana density $\mathcal{P}_M(45) = 10^{-9}$. At earlier stages, when the potential barrier is not high enough, these internal quasiparticle states overlap with each other significantly, being hardly detectable in the spectral function $\mathcal{P}_M(i)$ for $\tau \leq 45$. We hence conclude that the profiles of both the trapping potential and the internal scattering barrier must be carefully designed in order to achieve the zero-energy Majorana quasiparticles in the ultracold fermionic atom systems.

4. Summary

We investigated the possible realization of Majorana quasiparticles in a one dimensional trapped fermionic system, within the scenario proposed in [16]. Our study indicates that the MBS are very sensitive to the trapping potential, preferring its flat shapes. We have investigated this effect, plotting the phase diagram of the topological phase (characterized by a change of the parity \mathcal{Q}) with respect to the parameters of the (parabolic and Gaussian) trapping potentials. In practice, their profiles can be controllably designed by counter-propagating laser beams.

We analyzed the system in which one pair of Majorana quasiparticles initially exists. We also considered an internal quantum defect, which can create an additional pair of MBS in a continuous way, upon changing the height and width of the potential barrier, without disappearance of the initial one. This process should be feasible in ultracold gases by applying external laser beams. Similar effects might be also achieved in solid state realizations, with appropriate gating of individual sites in the proximitized superconducting nanowires [15]. We have shown that such additional scattering potential has to be large/wide enough in order to obtain the zero-energy Majorana quasiparticles. This could be important for future realizations of their braiding, using various interfaces of topological and non-topological superconducting regions.

Our study of internal MBS in ultracold gases could be interesting for the perspective of quantum computing [13, 109]. Two pairs of MBS with opposite polarizations [56] can be written/read without any risk of decoherence, because of their topological protection. If the saved information is copied into separate parts in the system, then information will survive in one of the qubits, while the second qubit can be used for additional quantum operations. Finally, the initial information can be confronted with results of computations performed in the meantime.

Acknowledgments

We thank Krzysztof Cichy for careful reading of the manuscript, valuable comments and discussions. We also thank

⁸The BdG equations have been solved by exact diagonalisation of the matrix (3) [110]. As a consequence, we must assume cut-off energy defining the 'numerical zero' energy, as $10^{-14}t$.

Ravindra Chhajlany, Jelena Klinovaja, Roman M Lutchyn, Maciej M Maška, Pascal Simon and Jakub Tworzydło for fruitful discussions. This work was supported by the National Science Centre (NCN, Poland) under grants UMO-2016/20/S/ST3/00274 (AP), UMO-2017/25/B/ST3/02586 (AP), UMO-2017/24/C/ST3/00357 (AC) and DEC-2014/13/B/ST3/04451 (TD).

ORCID iDs

Andrzej Ptok  <https://orcid.org/0000-0002-5566-2656>

References

- [1] Bloch I, Dalibard J and Nascimbene S 2012 *Nat. Phys.* **8** 267
- [2] Dalibard J, Gerbier F, Juzeliūnas G and Öhberg P 2011 *Rev. Mod. Phys.* **83** 1523
- [3] Bloch I, Dalibard J and Zwerger W 2008 *Rev. Mod. Phys.* **80** 885
- [4] Lin Y J, Compton R L, Jimenez-Garcia K, Porto J V and Spielman I B 2009 *Nature* **462** 628
- [5] Cheuk L W, Sommer A T, Hadzibabic Z, Yefsah T, Bakr W S and Zwierlein M W 2012 *Phys. Rev. Lett.* **109** 095302
- [6] Galitski V and Spielman I B 2013 *Nature* **494** 49
- [7] Williams R A, Beeler M C, LeBlanc L J, Jiménez-García K and Spielman I B 2013 *Phys. Rev. Lett.* **111** 095301
- [8] Huang L, Meng Z, Wang P, Peng P, Zhang S L, Chen L, Li D, Zhou Q and Zhang J 2016 *Nat. Phys.* **12** 540
- [9] Wu L N, Luo X Y, Xu Z F, Ueda M, Wang R and You L 2017 *Sci. Rep.* **7** 46756
- [10] Kitaev A Y 2001 *Phys.—Usp.* **44** 131
- [11] Wilczek F 2009 *Nat. Phys.* **5** 614
- [12] Leijnse M and Flensberg K 2012 *Semicond. Sci. Technol.* **27** 124003
- [13] Nayak C, Simon S H, Stern A, Freedman M and Das Sarma S 2008 *Rev. Mod. Phys.* **80** 1083
- [14] Stern A 2010 *Nature* **464** 187
- [15] Alicea J, Oreg Y, Refael G, von Oppen F and Fisher M P A 2011 *Nat. Phys.* **7** 412
- [16] Jiang L, Kitagawa T, Alicea J, Akhmerov A R, Pekker D, Refael G, Cirac J I, Demler E, Lukin M D and Zoller P 2011 *Phys. Rev. Lett.* **106** 220402
- [17] Mourik V, Zuo K, Frolov S M, Plissard S R, Bakkers E P A M and Kouwenhoven L P 2012 *Science* **336** 1003
- [18] Deng M T, Yu C L, Huang G Y, Larsson M, Caroff P and Xu H Q 2012 *Nano Lett.* **12** 6414
- [19] Das A, Ronen Y, Most Y, Oreg Y, Heiblum M and Shtrikman H 2012 *Nat. Phys.* **8** 887
- [20] Chang W, Albrecht S M, Jespersen T, Kuemmeth F, Krogstrup P, Nygård J and Marcus C M 2015 *Nat. Nanotechnol.* **10** 232
- [21] Albrecht S M, Higginbotham A P, Madsen M, Kuemmeth F, Jespersen T S, Nygård J, Krogstrup P and Marcus C M 2016 *Nature* **531** 206
- [22] Deng M T, Vaitiekenas S, Hansen E B, Danon J, Leijnse M, Flensberg K, Nygård J, Krogstrup P and Marcus C M 2016 *Science* **354** 1557
- [23] Gül O *et al* 2017 *Nano Lett.* **17** 2690
- [24] Nadj-Perge S, Drozdov I K, Li J, Chen H, Jeon S, Seo J, MacDonald A H, Bernevig B A and Yazdani A 2014 *Science* **346** 602
- [25] Ruby M, Pientka F, Peng Y, von Oppen F, Heinrich B W and Franke K J 2015 *Phys. Rev. Lett.* **115** 197204
- [26] Pawlak R, Kisiel M, Klinovaja J, Meier T, Kawai S, Glatzel T, Loss D and Meyer E 2016 *NPJ Quantum Inf.* **2** 16035

- [27] Ruby M, Heinrich B W, Peng Y, von Oppen F and Franke K J 2017 *Nano Lett.* **17** 4473
- [28] Feldman B E, Randeria M T, Li J, Jeon S, Xie Y, Wang Z, Drozdov I K, Andrei Bernevig B and Yazdani A 2017 *Nat. Phys.* **13** 286
- [29] Jeon S, Xie Y, Li J, Wang Z, Bernevig B A and Yazdani A 2017 *Science* **358** 772
- [30] Lin Y J, Jiménez-García K and Spielman I B 2011 *Nature* **471** 83
- [31] Wang P, Yu Z Q, Fu Z, Miao J, Huang L, Chai S, Zhai H and Zhang J 2012 *Phys. Rev. Lett.* **109** 095301
- [32] Fu L and Kane C L 2008 *Phys. Rev. Lett.* **100** 096407
- [33] Rakhmanov A L, Rozhkov A V and Nori F 2011 *Phys. Rev. B* **84** 075141
- [34] Biswas R R 2013 *Phys. Rev. Lett.* **111** 136401
- [35] Li Z Z, Zhang F C and Wang Q H 2014 *Sci. Rep.* **4** 6363
- [36] Sun H H et al 2016 *Phys. Rev. Lett.* **116** 257003
- [37] Suominen H J, Kjaergaard M, Hamilton A R, Shabani J, Palmstrøm C J, Marcus C M and Nichele F 2017 *Phys. Rev. Lett.* **119** 176805
- [38] Zhang C, Tewari S, Lutchyn R M and Das Sarma S 2008 *Phys. Rev. Lett.* **101** 160401
- [39] Sato M and Fujimoto S 2009 *Phys. Rev. B* **79** 094504
- [40] Sato M, Takahashi Y and Fujimoto S 2010 *Phys. Rev. B* **82** 134521
- [41] Seo K, Han L and Sá de Melo C A R 2012 *Phys. Rev. A* **85** 033601
- [42] Bühler A, Lang N, Kraus C, Möller G, Huber S and Büchler H 2014 *Nat. Commun.* **5** 4504
- [43] Zwierlein M W, Abo-Shaeer J R, Schirotzek A, Schunck C H and Ketterle W 2005 *Nature* **435** 1047
- [44] Zwierlein M W, Schirotzek A, Schunck C H and Ketterle W 2006 *Science* **311** 492
- [45] Partridge G B, Li W, Kamar R I, Liao Y A and Hulet R G 2006 *Science* **311** 503
- [46] Aidelsburger M, Atala M, Lohse M, Barreiro J T, Paredes B and Bloch I 2013 *Phys. Rev. Lett.* **111** 185301
- [47] Chin C and Mueller E J 2013 *Physics* **6** 118
- [48] Holland M, Kokkelmans S J J M F, Chiofalo M L and Walser R 2001 *Phys. Rev. Lett.* **87** 120406
- [49] de Gennes P G 1989 *Superconductivity of Metals and Alloys* (Reading, MA: Addison-Wesley)
- [50] Kinnunen J, Jensen L M and Törmä P 2006 *Phys. Rev. Lett.* **96** 110403
- [51] Baur S K, Basu S, De Silva T N and Mueller E J 2009 *Phys. Rev. A* **79** 063628
- [52] Yanase Y 2009 *Phys. Rev. B* **80** 220510
- [53] Baksmaty L O, Lu H, Bolech C J and Pu H 2011 *New J. Phys.* **13** 055014
- [54] Liu X J and Hu H 2012 *Phys. Rev. A* **85** 033622
- [55] Domański T 2011 *Phys. Rev. A* **84** 023634
- [56] Sticlet D, Bena C and Simon P 2012 *Phys. Rev. Lett.* **108** 096802
- [57] Akhmerov A R, Dahlhaus J P, Hassler F, Wimmer M and Beenakker C W J 2011 *Phys. Rev. Lett.* **106** 057001
- [58] Matsui H, Sato T, Takahashi T, Wang S C, Yang H B, Ding H, Fujii T, Watanabe T and Matsuda A 2003 *Phys. Rev. Lett.* **90** 217002
- [59] Okazaki K et al 2014 *Sci. Rep.* **4** 4109
- [60] Rainis D, Trifunovic L, Klinovaja J and Loss D 2013 *Phys. Rev. B* **87** 024515
- [61] Liu C X, Sau J D, Stanescu T D and Das Sarma S 2017 *Phys. Rev. B* **96** 075161
- [62] Ptok A, Kobińska A and Domański T 2017 *Phys. Rev. B* **96** 195430
- [63] Prada E, Aguado R and San-Jose P 2017 *Phys. Rev. B* **96** 085418
- [64] Szumniak P, Chevallier D, Loss D and Klinovaja J 2017 *Phys. Rev. B* **96** 041401
- [65] Chevallier D, Szumniak P, Hoffman S, Loss D and Klinovaja J 2018 *Phys. Rev. B* **97** 045404
- [66] Hell M, Flensberg K and Leijnse M 2018 *Phys. Rev. B* **97** 161401
- [67] Dutta O, Gajda M, Hauke P, Lewenstein M, Lühmann D S, Malomed B A, Sowiński T and Zakrzewski J 2015 *Rep. Prog. Phys.* **78** 066001
- [68] Regal C A, Ticknor C, Bohn J L and Jin D S 2003 *Nature* **424** 47
- [69] Moritz H, Stöferle T, Günter K, Köhl M and Esslinger T 2005 *Phys. Rev. Lett.* **94** 210401
- [70] Shin Y, Schunck C H, Schirotzek A and Ketterle W 2007 *Phys. Rev. Lett.* **99** 090403
- [71] Stewart J T, Gaebler J P and Jin D S 2008 *Nature* **454** 744
- [72] Fröhlich B, Feld M, Vogt E, Koschorreck M, Zwerger W and Köhl M 2011 *Phys. Rev. Lett.* **106** 105301
- [73] Törmä P 2016 *Phys. Scr.* **91** 043006
- [74] Kinnunen J, Rodríguez M and Törmä P 2004 *Science* **305** 1131
- [75] Chin C, Bartenstein M, Altmeyer A, Riedl S, Jochim S, Denschlag J H and Grimm R 2004 *Science* **305** 1128
- [76] Bena C 2017 *C. R. Phys.* **18** 349
- [77] Zhang P and Nori F 2016 *New J. Phys.* **18** 043033
- [78] Kane C L and Mele E J 2005 *Phys. Rev. Lett.* **95** 146802
- [79] Fulga I C, Hassler F, Akhmerov A R and Beenakker C W J 2011 *Phys. Rev. B* **83** 155429
- [80] Moore J E and Balents L 2007 *Phys. Rev. B* **75** 121306
- [81] Qi X L, Hughes T L and Zhang S C 2008 *Phys. Rev. B* **78** 195424
- [82] Roy R 2009 *Phys. Rev. B* **79** 195322
- [83] Hasan M Z and Kane C L 2010 *Rev. Mod. Phys.* **82** 3045
- [84] Qi X L and Zhang S C 2011 *Rev. Mod. Phys.* **83** 1057
- [85] Altland A and Zirnbauer M R 1997 *Phys. Rev. B* **55** 1142
- [86] Ryu S, Schnyder A P, Furusaki A and Ludwig A W W 2010 *New J. Phys.* **12** 065010
- [87] Schnyder A P, Ryu S, Furusaki A and Ludwig A W W 2008 *Phys. Rev. B* **78** 195125
- [88] Sato M, Takahashi Y and Fujimoto S 2009 *Phys. Rev. Lett.* **103** 020401
- [89] Shin Y, Zwierlein M W, Schunck C H, Schirotzek A and Ketterle W 2006 *Phys. Rev. Lett.* **97** 030401
- [90] Orso G 2007 *Phys. Rev. Lett.* **98** 070402
- [91] Hu H, Liu X J and Drummond P D 2007 *Phys. Rev. Lett.* **98** 070403
- [92] Amaricci A, Privitera A and Capone M 2014 *Phys. Rev. A* **89** 053604
- [93] Liu X J and Drummond P D 2012 *Phys. Rev. A* **86** 035602
- [94] Xu Y, Mao L, Wu B and Zhang C 2014 *Phys. Rev. Lett.* **113** 130404
- [95] Liu X J 2015 *Phys. Rev. A* **91** 023610
- [96] Butts D A and Rokhsar D S 1997 *Phys. Rev. A* **55** 4346
- [97] San-Jose P, Cayao J, Prada E and Aguado R 2016 *Sci. Rep.* **6** 21427
- [98] Potter A C and Lee P A 2010 *Phys. Rev. Lett.* **105** 227003
- [99] Mishmash R V, Aasen D, Higginbotham A P and Alicea J 2016 *Phys. Rev. B* **93** 245404
- [100] DeGottardi W, Sen D and Vishveshwara S 2011 *New J. Phys.* **13** 065028
- [101] Kundu A and Seradjeh B 2013 *Phys. Rev. Lett.* **111** 136402
- [102] Liu D E, Levchenko A and Baranger H U 2013 *Phys. Rev. Lett.* **111** 047002
- [103] Hegde S, Shivamoggi V, Vishveshwara S and Sen D 2015 *New J. Phys.* **17** 053036
- [104] Potter A C, Morimoto T and Vishwanath A 2016 *Phys. Rev. X* **6** 041001
- [105] Souto R S, Martín-Rodero A and Yeyati A L 2016 *Phys. Rev. Lett.* **117** 267701
- [106] Liu D E, Levchenko A and Lutchyn R M 2017 *Phys. Rev. B* **95** 115303
- [107] Chevallier D, Sticlet D, Simon P and Bena C 2012 *Phys. Rev. B* **85** 235307
- [108] Chevallier D, Simon P and Bena C 2013 *Phys. Rev. B* **88** 165401
- [109] Rainis D and Loss D 2012 *Phys. Rev. B* **85** 174533
- [110] Ptok A and Kapcia K J 2015 *Supercond. Sci. Technol.* **28** 045022